Electronic structures of C_{60} and C_{70} adsorbed on the Cu(111) surface and intramolecular STM images

Yutaka Maruyama, Kaoru Ohno, and Yoshiyuki Kawazoe
Institute for Materials Research, Tohoku University, Sendai 980-77, Japan
(Received 8 November 1994; revised manuscript received 24 March 1995)

Recent scanning tunneling microscopy (STM) experiments have revealed that C_{60} and C_{70} adsorbed on the Cu(111)-(1×1) substrate show specific bias-voltage-dependent images that seem to reflect individual cage structures. In order to understand this experimental observation, band structures and partial charge-density distributions of C_{60} and C_{70} are calculated by means of an all-electron mixed-basis approach. In this paper we adopt two-dimensional molecular models without substrates and proper orientational adsorption geometries of fullerenes. By comparing the calculated charge distributions of the lowest-unoccupied-molecular-orbital bands and the highest-occupied-molecular-orbital bands with the STM images, we find that the intramolecular patterns that change with the bias voltage strongly reflect the positions of five-membered and six-membered rings.

I. INTRODUCTION

In the past decade, after the discovery of C_{60} by Kroto *et al.*[1] in 1985, fullerenes have attracted much interest among various research fields. One of the current interests is the mechanism of nucleation and growth of fullerene thin film and its adsorption structure on substrate. Concerning the behaviors of fullerenes on the substrate, it is very important to understand how fullerenes interact with the substrate and with each other. So far, an anomalous amount of experimental efforts have been devoted to this field. Among them the scanning tunneling microscopy (STM) is a powerful technique in the direct imaging of fullerenes on an atomic scale. According to the STM observations, fullerenes interact with substrates and align commensurately on various substrates, such as HOPG,[2] GaAs,[3] Si,[4,5] Ag,[6] Au,[7] and Cu.[8–10] On the Au(111) and Cu(111) surfaces it is especially known that both C_{60} and C_{70} form ideal triangular lattices in the first layer. Furthermore, several experimental groups have reported the observation of intramolecular patterns that seem to reflect the cage structures composed of five-membered and six-membered rings in C_{60}, C_{70}, and C_{84}. For example, C_{60}'s adsorbed on the Au(110) surface show images of rings surrounded by six or five spots;[7] C_{60}'s adsorbed on the Si(100) (Refs. 5 and 12) and Si(111)7×7 (Ref. 11) surfaces show mainly four stripes running in parallel; C_{70}'s adsorbed on the Au(110) surface[7] and C_{84}'s adsorbed on the Si(100) (Ref. 5) both contain internal patches that consist of several stripes and spots. The observation of the intramolecular patterns means that fullerenes are frozen on the surfaces because of the interactions with the substrate and with each other. This is interesting because fullerenes are known to be rotating in bulk crystals even at room temperature. More recently, Hashizume *et al.* have succeeded in observing specific intramolecular patterns, which depend on the bias voltage in pure C_{60} (Refs. 8 and 9) and C_{60}-C_{70} mixtures[10] adsorbed on the Cu(111) surface by using STM. At a positive bias voltage (with respect to the Fermi level), the images of individual C_{60} molecules appear as a three-leaf-clover shape. At a negative bias voltage, it changes to a doughnut shape. In a monolayer film composed of a C_{60}-C_{70} mixture, C_{70} is observed more brightly than C_{60} and has two types of shapes; one is round with no intramolecular pattern and the other has an intramolecular pattern, which depends weakly upon the bias voltage: at positive bias voltage, individual C_{70} shows two parallel spots or a rectangular spot with an inscribed cross.

Although experimental studies have revealed many specific images of fullerenes adsorbed on various surfaces, only few theoretical attempts have been made to explain these images.[12,13] It is very important to consider the specific internal patterns, especially in relation to both the electronic structure and the adsorption configuration, since the STM typically images a spatial distribution of the local density of states near the Fermi level through the tunneling current.

In this study, we focus on C_{60} and C_{70} adsorbed on the Cu(111) surface and investigate the origin of specific STM images and their bias-voltage dependence by performing first-principle band calculations. X-ray photoemission spectroscopy and high-resolution electron-energy-loss spectroscopy experiments on C_{60} adsorbed on the Cu substrate[14] have revealed that the Cu substrate plays a role similar to that of K in K_3C_{60} and donates electrons to fill the lowest-unoccupied-molecular-orbital (LUMO) band. Moreover, the amount of charge transfer from the Cu substrate to C_{60} is about one electron per C_{60} molecule, which is less than in the case of K_3C_{60}. Here, we take for granted that the amount of electron charge transfer from the Cu substrate to the fullerenes does not affect the band structure and only shifts the energy levels, i.e., we assume that the so-called rigid-band picture holds. We checked that this is a reasonable approximation in the present case. Therefore, we adopt a simple model that the Cu substrate affects fullerenes through an adsorption structure only. In this model, we assume suitable adsorption

0163-1829/95/52(3)/2070(6)/$06.00 ©1995 The American Physical Society

geometries by taking account of the adsorption structures and the intramolecular images observed in experiments. This paper is organized as follows: In Sec. II the method of the present calculation is given, Sec. III introduces the model structure, in Sec. IV calculated results and discussions are presented, and our conclusion is stated in Sec. V.

II. METHOD OF CALCULATION

When one treats a system that includes first-row elements, such as carbon, by the conventional plane-wave expansion method, a huge number of basis functions is required to represent accurately the behavior of the wave functions in the core region. Therefore, in the present study, we adopt a mixed-basis approach, which was originally introduced by Louie, Ho, and Cohen[15] in order to treat localized d orbitals within the pseudopotential formalism. The present method, however, is not a straight extension of their work and should be regarded as a fundamentally different approach in the sense that we treat all electrons including the $1s$ core state without using a pseudopotential. It enables us to express efficiently the spatial locality and asymmetry of the wave functions with a limited number of basis functions. This method has already been described elsewhere,[12] and here we briefly show the main points of the method.

A basis set consists of plane waves,

$$\frac{1}{\sqrt{\Omega}} e^{i(\mathbf{k}+\mathbf{G})\cdot\mathbf{r}} , \tag{1}$$

and Bloch sums of localized functions,

$$\Phi_{i\mu}(\mathbf{k},\mathbf{r})=\frac{1}{\sqrt{\Omega}} \sum_{\mathbf{R}_m} e^{i\mathbf{k}\cdot(\mathbf{R}_m+\tau_i)} \cdot f_{i\mu}(\mathbf{r}-\mathbf{R}_m-\tau_i) , \tag{2}$$

where $\mathbf{G}$ is a reciprocal-lattice vector, $\mathbf{R}_m$ a primitive vector, τ_i a basis vector, μ a label of the orbital on the ith atom, and Ω the crystal volume. In the present formulation, $1s$ and $2p$ Slater-type atomic orbitals are adopted as localized functions $f_{i\mu}(\mathbf{r})$. The exponential damping factors in $f_{i\mu}(\mathbf{r})$ are chosen so as not to overlap with neighboring localized functions.

The electron wave function is expressed by the sum of Eqs. (1) and (2) as

$$\psi_{\mathbf{k}}(\mathbf{r})=\frac{1}{\sqrt{\Omega}} \sum_{\mathbf{G}} A(\mathbf{k}+\mathbf{G}) e^{i(\mathbf{k}+\mathbf{G})\cdot\mathbf{r}} + \sum_{i\mu} B_{i\mu}(\mathbf{k}) \Phi_{i\mu}(\mathbf{k},\mathbf{r}) . \tag{3}$$

Since the localized functions are not orthogonal with the plane waves, a modified equation, which guarantees the orthogonality, becomes

$$H\Psi_{\mathbf{k}}=\epsilon_{\mathbf{k}} S \Psi_{\mathbf{k}} , \tag{4}$$

where S is the overlap matrix of the basis functions. This generalized eigenvalue problem is solved here by using a conventional Cholesky-decomposition-Householder scheme.

The effective one-electron Hamiltonian expressed in atomic units has the general form

$$H=T+V, \quad T=-\tfrac{1}{2}\nabla^2 , \tag{5}$$

$$V(\mathbf{r})=-\sum_n \frac{Z_n}{|\mathbf{r}-\mathbf{R}_n|} + \int dr' \frac{\rho(\mathbf{r}')}{|\mathbf{r}-\mathbf{r}'|} + V_{\mathrm{xc}}(\mathbf{r}) , \tag{6}$$

where $V_{\mathrm{xc}}(\mathbf{r})$ is the local exchange-correlation potential that is evaluated in real space using the local-density approximation. In the present paper, V_{xc} is approximated by the $X\alpha$ method;

$$V_{\mathrm{xc}}(\mathbf{r})=-3\alpha \left[\frac{3}{8\pi} \rho(\mathbf{r}) \right]^{1/3} , \tag{7}$$

where $\alpha=0.9$ is adopted for the exchange-correlation parameter.

III. MODEL STRUCTURE AND CHARGE DISTRIBUTION

In this paper we investigate the relationship among the specific internal patterns observed in fullerenes, the electronic structures, and the orientational adsorption geometries. To this purpose, we compare the computed charge-density distributions of fullerenes with the observed STM images.

First of all, we have to pay attention to the model structure, since it is not clear what orientational geometries should be chosen at the outset. C_{60} and C_{70} have several possible adsorption geometries, because of their unique cage structures: C_{60} has a spherical cage structure with I_h symmetry, which consists of 12 five-membered rings and 20 six-membered rings, while C_{70} has an ellipsoidal cage structure with D_{5h} symmetry, which consists of 12 five-membered rings and 25 six-membered rings.

Figures 1(a) and 1(b) show two model structures adopted in this study. As is discussed below, they correspond to the pure C_{60} and the C_{60}-C_{70} mixture, respectively, adsorbed on the Cu(111) surface. The areas which are enclosed with solid lines represent unit cells. [Below, charge-density distributions of C_{60} will be shown only for half of the unit cell as indicated in Fig. 1(a).]

In the case of pure C_{60}'s, we adopt the ideal triangular lattice as the adsorption structure. The orientational adsorption geometries were determined by taking into account the relationship between the adsorption structure and the observed three-leaf-clover pattern as follows:

Case A. C_{60} forms the ideal triangular lattice with a lattice constant 10.2 Å. One of the six-membered rings in C_{60} is at the topmost position and parallel to the crystal plane. (Opposite six-membered ring is at the lowest position.) Three five-membered rings around the topmost six-membered ring form a small regular triangle, whose vertices face the neighboring C_{60}.

In this orientation of C_{60}, the lateral five-membered ring faces the six-membered ring of the neighboring C_{60} and vice verse. Taking into account that five-membered rings are charge-poor and six-membered rings are charge rich, this orientation seems to be energetically favorable, because of the minimum overlap of electronic clouds.

In the case of pure C_{70}, it is known that C_{70} takes "a

standing shape" (long-axis perpendicular to the substrate), which shows the spherical pattern without internal structure and results in the ideal triangular lattice.[10] In the case of C_{60}-C_{70} mixture, however, the neighboring C_{60}'s play an important role in the orientation of C_{70}. C_{70} can take "a laying-down shape" (long-axis parallel to the substrate) and shows the intramolecular pattern such as the rectangular spot with an inscribed cross [see Fig. 3(a) of Ref. 10]. This spot clearly depends on the configurations of neighboring fullerenes. We have considered the two-dimensional (2D) crystal, which consists of a pair of C_{60} and C_{70} represented periodically. The orientation of C_{70} was determined by taking account of the images showing the rectangular spot with an inscribed cross and the configuration of neighboring C_{60}. In the STM picture, C_{70} is observed more brightly than C_{60}. This is a curious aspect, because the laying-down C_{70} has almost the same diameter in the shorter equator as C_{60}. Below, in our model, we assume that the distances of C_{60} and C_{70} from the substrate are the same.

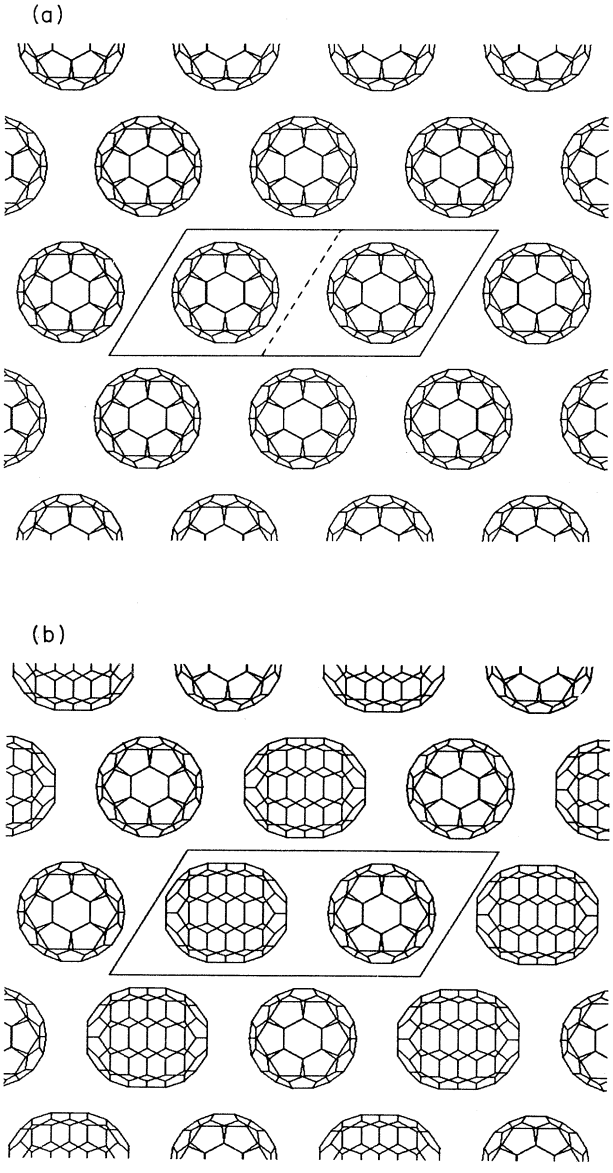

FIG. 1. Model structures and the unit cells of (a) C_{60} monolayer (case *A*), and (b) C_{60}-C_{70} mixture monolayer (case *B*).

Case B. (b) C_{70} and C_{60} are alternatively arranged in one direction. Each C_{60} is oriented as in case *A*, while each C_{70} is oriented as follows: one of the six-membered rings in C_{70}, whose center is located on the shorter equator, is at the lowest position and parallel to the crystal plane corresponding to the substrate. In this orientation, a 6/6 bond along the shorter equator comes to the topmost position and the two six-membered rings sharing this bond are along with the topmost longer equator; four five-membered rings are located adjacent, i.e., at the four corners in the topview of C_{70}, and the long axis of C_{70} points to the neighboring C_{60}'s. Every intermolecular distance is 10.2 Å.

As for intramolecular bond lengths, we adopt two C-C lengths in both C_{60} and C_{70} cages, i.e., 1.46 Å for all the bond belonging to five-membered rings and 1.40 Å for all the 6/6 bonds.

As mentioned above, the STM observes the tunneling current, which strongly depends on both the electronic structure and the atomic configuration. More precisely, the tunneling current should be determined by the specimen and the tip of the STM. Detailed works on the comparison between the calculated images and the STM images have already been performed.[16,17] Although these offer us some accurate information, instead, we simply assume that the STM images are approximated by partial charge distributions only. These charge distributions, which should be compared with the STM images, are obtained by adding up several levels around the highest-occupied-molecular-orbital–(HOMO-) LUMO gap with the same weight. In case *A*, the charge distributions are calculated in half the unit cell and the band structure is calculated in the unit cell that contains two C_{60}'s. In case *B*, both the charge distribution and the band structure are calculated in the unit cell, which contains C_{60} and C_{70}. Since the size of the Brillouin zone is small and the system has predominantly a molecular character for fullerenes, we calculate the potential and the charge density by using the Γ point only.

IV. RESULTS AND DISCUSSION

The present result of the band energy dispersion of case *A* is shown in Fig. 2(a), which contains 100 levels around the HOMO-LUMO gap. The value of the band gap is calculated to be 1.2 eV, which is larger than the previous result of 1.1 eV, for the case of the fcc ($Fm\bar{3}$) symmetry.[18] Other basic features are almost similar to the 3D crystal band structures. Globally, there are two types of bands. One is an intramolecular σ band, which has no dispersion. The other is an intermolecular band, which has relatively strong dispersion. In either case, it is found that the dispersion is not strong enough to mix up energy levels over forbidden gaps of the isolated molecule. This indicates that each band keeps its original molecular character, such as h_u (HOMO) and t_{1u} (LUMO).

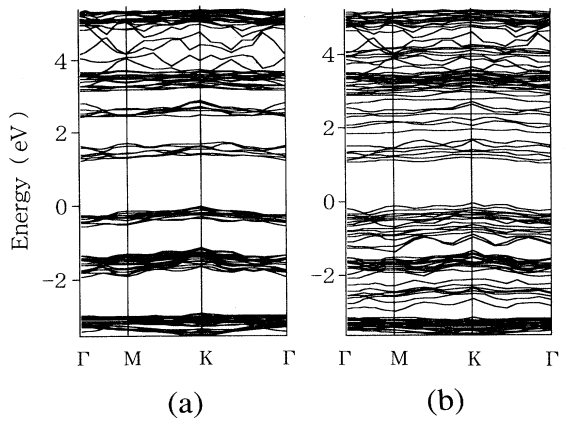

FIG. 2. Band energy dispersions of (a) C_{60} monolayer (case *A*) and (b) C_{60}-C_{70} mixture monolayer (case *B*).

The STM theory shows that bands that are located near the Fermi level mainly contribute to the tunneling current. However, it is impossible to determine the Fermi level, which depends on the amount of charge transfer from the Cu substrate to the C_{60} monolayer, within the framework of the present model. We determined the number of bands that should be added up so as to include all of the bands that have the same symmetry character in the molecule: (a) Three LUMO bands, (b) five HOMO bands are added up, respectively.

The calculated partial charge distributions are shown in Fig. 3. The isosurface of charge density at 0.005 $Å^{-3}$ is drawn in the figure. Figure 3(a) shows that the three five-membered rings around the topmost six-membered ring are highlighted just like a three-leaf clover. Figure 3(b) shows that the topmost six-membered ring is highlighted with a center hole just like a doughnut. The present calculations reproduce the main features of the STM images observed in experiments. The specific STM image observed at the positive bias voltage corresponds to the charge distribution of the LUMO bands. The tunneling current flows from the STM tip to the electronic states of the LUMO bands, which are mainly located on single bonds, and hence the five-membered rings, which consist of single bonds, are highlighted. On the other hand, the charge distribution of the HOMO bands is observed when the bias voltage is negative. The tunneling current flows from the electronic states of the HOMO bands, which are mainly located on double bonds to the STM tip, therefore, the six-membered ring is highlighted.

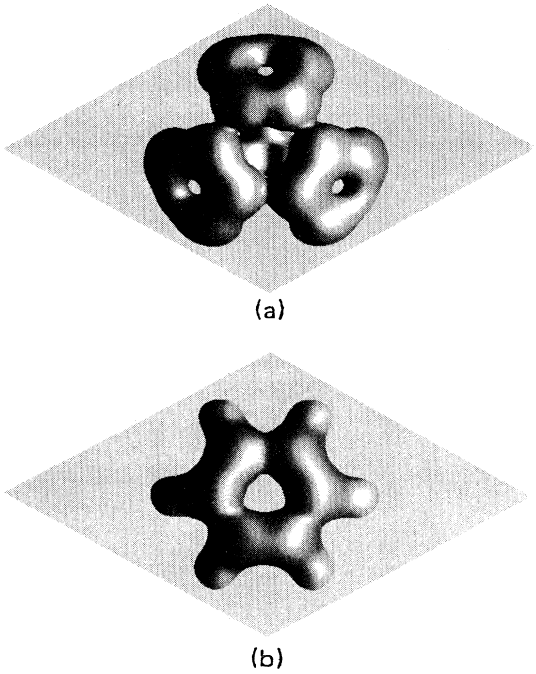

FIG. 3. Calculated charge distributions of C_{60} monolayer (case *A*); (a) LUMO bands and (b) HOMO bands.

The calculated band energy dispersion of case *B* is shown in Fig. 2(b), which contains 100 levels around the HOMO-LUMO gap. By comparing the band structures of cases *A* and *B*, it is found that many degeneracies disappear in case *B*, because of the lower symmetry of C_{70}. We find that the levels in case *B*, which occur in the forbidden gaps in case *A*, are mainly due to C_{70}. The HOMO-LUMO gap in case *B* is given by $E_g \sim 1.0$ eV, which is smaller than 1.2 eV for case *A*, because (i) the intrinsic band gap of C_{70} is narrower than C_{60},[19–21] and (ii) the interatomic distance between C_{60} and C_{70} is shorter than that of pure C_{60}'s.

Similar to case *A*, the dispersion is not strong enough to mix up the bands that have different characters, and forbidden gaps that exist in isolated molecules remain in the crystalline phase. We use the same strategy to make up the charge distributions. By taking account of the above band structure, (a) six LUMO bands were added up (half of them come from C_{70}), (b) 15 HOMO bands were added up (ten bands associated with C_{70}).

The calculated partial charge distributions are shown in Fig. 4, where the isosurface of charge density at 0.005 $Å^{-3}$ is drawn. In (a) the charge distribution of the

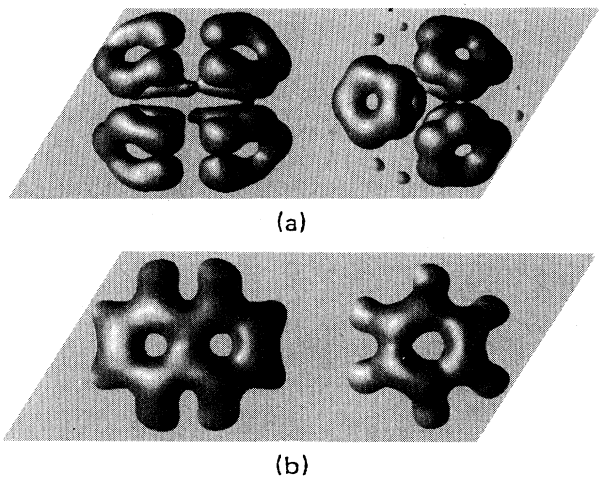

FIG. 4. Calculated charge distributions of C_{60}-C_{70} mixture monolayer (case *B*); (a) LUMO bands and (b) HOMO bands.

LUMO bands, three five-membered rings around the six-membered ring in C_{60} are highlighted like in case *A*, and four five-membered rings in C_{70} are highlighted with two mirror surfaces just like the observed STM image. In (b) the charge distribution of the HOMO bands, the topmost six-membered ring of C_{60}, and the topmost 6/6 bond and upper six-membered rings in C_{70} are highlighted.

We find a good agreement between the STM image observed at positive bias voltage and the charge distribution of the LUMO bands. The charge distribution of the HOMO bands is compared with the STM image that was observed at negative bias voltage [see Fig. 3(b) of Ref. 10]. The calculated charge distribution Fig. 4(b) and the observed STM image have basically similar shapes and the agreement is very good. However, one may additionally find an asymmetry along the long axis of C_{70} in the STM image observed at the negative bias voltage, which was absent at the positive bias voltage. We cannot find such an asymmetry in our Fig. 4(b), which is obtained by adding the 15 HOMO bands. When we change the number of levels from 1 to 14, which are added to make the HOMO-charge distributions, we do have an asymmetric charge distribution, but with asymmetries along the short axis of C_{70}, which are different from the STM image. Even if some doubts remain about the detailed patterns, it is clear that the assumed orientational adsorption geometry reproduces the main features observed experimentally.

Finally, we briefly comment on the difference in brightnesses observed in C_{60} and in C_{70}. One possibility to explain the difference is that the LDOS is higher in C_{70} than C_{60}. However, we could not recognize a distinct difference in the charge distribution between C_{60} and C_{70}. In the present geometry, C_{60} faces the Cu surface with the six-membered ring neighboring to three five-membered rings, and C_{70} faces the surface with the six-membered ring neighboring to two five-membered rings. This difference of the number of the neighboring five-membered rings might cause a difference in the adsorption interaction, and in turn a difference in the distance from the substrate. To reproduce this difference and the detailed feature mentioned above, the STM tip interaction and the effect of the substrate must be explicitly taken into account.

V. CONCLUSION

In this study, we have performed band-structure calculations of C_{60} and C_{60}-C_{70} mixture monolayers in order to understand the bias-voltage-dependent intramolecular patterns observed in C_{60} and C_{70} adsorbed on the Cu(111)-(1×1) surface. We adopted simple models, which assumed the 2D crystal structure and the proper orientational adsorption geometry. The computed energy-band dispersions represent the specific symmetric features of the molecular C_{60} and C_{70}, because the intermolecular distance of fullerenes (10.2 Å) is large enough to separate the adsorbed fullerenes, and hence their original levels remain.

By comparing the calculated charge distributions with the observed STM images, we have found that the highlighted regions of the STM images at the positive and negative bias voltages are, respectively, described by the LUMO and HOMO bands and correspond to the positions of five- and six-membered rings. That is, the patterns strongly depend on the orientation of the fullerenes. The three-leaf-clover shape observed on C_{60}, at the positive bias voltage, corresponds to the three five-membered rings around the topmost six-membered ring of C_{60}. The doughnut shape observed at the negative bias voltage corresponds to the topmost six-membered ring. The rectangular spot with an inscribed cross in C_{70} observed at the positive bias voltage corresponds to the four five-membered rings.

ACKNOWLEDGMENTS

The authors would like to express their sincere thanks to Professor Sakurai, Dr. Hashizume, and Professor Bing-lin Gu for their valuable discussions and comments. They are also grateful to IBM Japan Co. for the partnership program on materials design by computer. This work has been supported in part by the Grant-in-Aid of the priority area "Carbon Cluster" from the Ministry of Education, Science and Culture. The HITAC S-3800/380 supercomputer facilities used are maintained by the Computer Science Group of the Institute. They would also like to thank Professor Marcel Sluiter and Dr. Keivan Esfarjani for their careful reading of the manuscript.

[1]H. W. Kroto, J. R. Heath, S. C. O'Brien, R. E. Curl, and R. E. Smalley, Nature (London) **318**, 162 (1985).

[2]J. L. Wragg, J. E. Chamberlain, H. W. White, W. Kratschmer, and D. R. Huffman, Nature (London) **348**, 623 (1990).

[3]Y. Z. Li, J. C. Patrin, M. Chander, J. H. Weaver, L. P. F. Chibante, and R. E. Smalley, Nature (London) **252**, 547 (1991).

[4]Y. Z. Li, M. Chander, J. C. Patrin, J. H. Weaver, L. P. F. Chibante, and R. E. Smalley, Phys. Rev. B **45**, 13 837 (1992).

[5]X.-D. Wang, T. Hashizume, H. Shinohara, Y. Saito, Y. Nishina, and T. Sakurai, Phys. Rev. B **47**, 15 923 (1993).

[6]T. David, J. K. Gimezewski, D. Purdie, B. Reihl, and R. R. Schlittler, Phys. Rev. B **50**, 5810 (1994).

[7]Yun Zhang, Xiaoping Gao, and Michael J. Weaver, J. Phys. Chem. **96**, 510 (1992).

[8]T. Hashizume, K. Motai, X.-D. Wang, H. Shinohara, Y. Saito, Y. Maruyama, K. Ohno, Y. Kawazoe, Y. Nishina, H. W. Pickering, Y. Kuk, and T. Sakurai, Phys. Rev. Lett. **71**, 2959 (1993).

[9]Kumi Motai, Tomihoro Hashizume, Hisanori Shinohara, Yahachi Sito, Howard W. Pickering, Yuichiro Nishina, and Toshio Sakurai, Jpn. J. Appl. Phys. **32**, 450 (1993).

[10]X.-D. Wang, V. Yu. Yurov, T. Hashizume, H. Shinohara, and T. Sakurai, Phys. Rev. B **49**, 14 746 (1994).

[11]Xian-Dong Wang, Tomihiro Hashizume, Hisanori Shinohara, Yahachi Saito, Yuichiro Nishina, and Toshio Sakurai, Jpn. J. Appl. Phys. **31**, 983 (1992).

[12]Yoshiyuki Kawazoe, Hiroshi Kamiyama, Yutaka Maruyama, and Kaoru Ohno, Jpn. J. Appl. Phys. **32**, 1433 (1993).
[13]T. Yamaguchi and N. Fujima (unpublished).
[14]J. E. Rowe, P. Rudolf, L. H. Tjeng, R. A. Malic, G. Meigs, C. T. Chen, J. Chen, and E. W. Plummer, Int. J. Mod. Phys. B **6**, 3909 (1992).
[15]S. G. Louie, K. M. Ho, and M. L. Cohen, Phys. Rev. B **19**, 1774 (1979).
[16]J. Tersoff and D. R. Hammann, Phys. Rev. Lett. **20**, 1998 (1983).
[17]H. Kobayashi and M. Tsukada, Phys. Rev. B **46**, 6928 (1992).
[18]Bing-Lin Gu, Yutaka Maruyama, Jing-Zhi Yu, Kaoru Ohno, and Yoshiyuki Kawazoe, Phys. Rev. B **49**, 16 202 (1994).
[19]M. B. Jost, P. J. Benning, D. M. Poirier, J. H. Weaver, L. P. F. Chibante, and R. E. Smally, Chem. Phys. Lett. **184**, 423 (1991).
[20]J. H. Weaver, J. Chem. Solid **53**, 1433 (1992).
[21]K. Ohno, J.-Z. Yu, Y. Maruyama, Y. Kawazoe, and T. Takahashi (unpublished).

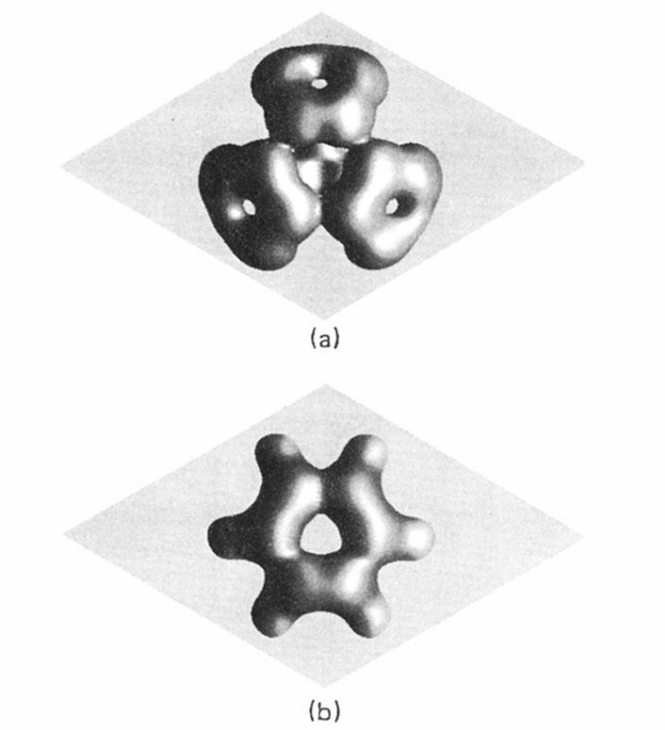

FIG. 3. Calculated charge distributions of C_{60} monolayer (case *A*); (a) LUMO bands and (b) HOMO bands.

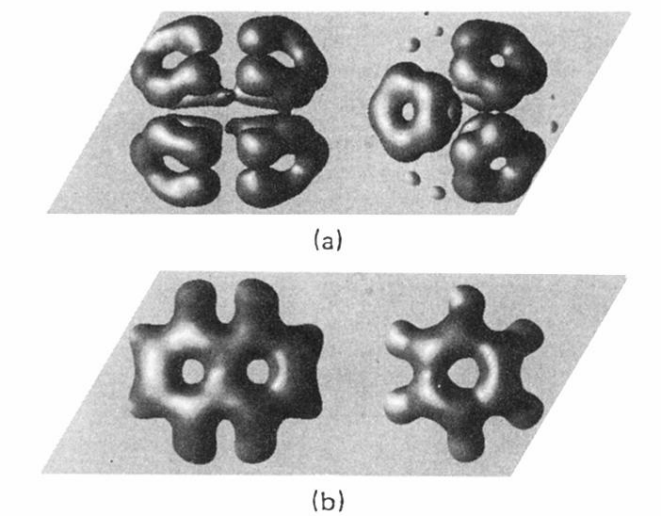

FIG. 4. Calculated charge distributions of C_{60}-C_{70} mixture monolayer (case *B*); (a) LUMO bands and (b) HOMO bands.